SCIENCE CHINA
Information Sciences

• RESEARCH PAPER •

January 2024, Vol. 67, Iss. 1, 112406:1–112406:11
https://doi.org/10.1007/s11432-023-3746-8

In situ plasmonic & electrochemical fiber-optic sensor for multi-metal-ions detection

Xiaoling PENG[1,2†], Zhiyong YANG[1†], Bo PENG[3*], Zhi LI[1], Zhicong REN[1], Xicheng WANG[1], Jiahai LI[1], Zhencheng LI[1], Liang CHEN[1], Daotong YOU[1], Kaiwei LI[4*], Jianqing LI[2*] & Tuan GUO[1*]

[1]*Institute of Photonics Technology, Jinan University, Guangzhou* 511443*, China;*
[2]*School of Computer Science and Engineering, Macau University of Science and Technology, Macao* 999078*, China;*
[3]*Institute for Environmental and Climate Research, Jinan University, Guangzhou* 511443*, China;*
[4]*Key Laboratory of Bionic Engineering of Ministry of Education, Jilin University, Changchun* 130022*, China*

Received 2 February 2023/Revised 18 March 2023/Accepted 13 April 2023/Published online 18 December 2023

Abstract High precision and high throughput detection of heavy metal ions is essential for water quality monitoring and assessment. Herein, we propose a plasmonic & electrochemical dual-mode fiber sensing probe for label-free and real-time detection of multiple ions (Pb^{2+} and Cu^{2+} as examples). This sensor comprises a multimode fiber-single mode fiber reflection probe, the outer surface of which is coated with a gold nanofilm to excite the surface plasmon resonance (SPR) optically and simultaneously serves as an electrochemical working electrode. In traditional electrochemical detection, the enrichment of ions cannot be detected in real-time. However, by utilizing the plasmonic & electrochemical dual-mode detection method, various kinds of metal ions can be deposited onto the gold nanofilm and selectively oxidized during forward potential scanning, and the entire electrochemical process can be monitored by SPR measurement. We experimentally demonstrate that the sensor can simultaneously detect Pb^{2+} and Cu^{2+} in a mixed solution in real-time, providing a linear response over the ion concentration range from 10^{-12} to 10^{-7} M and offering an excellent detection limit (1.69×10^{-14}–5.49×10^{-13} M). The proposed dual-mode fiber sensor has the benefits of remote sensing, compact footprint, and cost-effectiveness and shows excellent potential for water quality risk management in difficult-to-reach environments.

Keywords optical fiber sensor, surface plasmon resonance, electrochemical measurement, ions detection, water pollution

1 Introduction

Heavy metals are one of the most severe threats to the current ecosystems of humans, aquatic life, and animals of all inorganic pollutants found in nature [1]. Lead and copper ions (Pb^{2+} and Cu^{2+}) are two common heavy metal ions. Of these, Pb^{2+} can cause severe illness and even death at low levels of exposure, and Cu^{2+} is essential for human body functions but toxic in excess. These two heavy metals can migrate and accumulate in living tissues and may cause fatal diseases such as anemia, skeletal abnormalities, Alzheimer's/Wilson's disease, neurological disorders, and organ damage [2–4]. The maximum permitted levels for Cu^{2+} and Pb^{2+}, according to the United States Environmental Protection Agency (EPA), are 20 μM and 10 nM, respectively [5]. Therefore, sensitive, convenient, and low-cost detection of Pb^{2+} and Cu^{2+} in water samples is essential for water quality assessment.

Traditional analytical methods, such as cold vapor atomic absorption spectroscopy (CVAAS) [6], fluorescence spectrophotometry [7, 8], inductively coupled plasma atomic emission spectroscopy (ICP-AES) [9], and inductively coupled plasma mass spectrometry (ICP-MS) [10, 11], offer the advantages of high accuracy and sensitivity. These detection techniques, however, are costly, time-consuming, and complicated to operate, and more importantly, they cannot conduct *in situ* real-time inspections [5,12,13].

* Corresponding author (email: pengbo@jnu.edu.cn, kaiwei_li@jlu.edu.cn, jqli@must.edu.mo, tuanguo@jnu.edu.cn)
† Peng X L and Yang Z Y have the same contribution to this work.

The electrochemical detection method is extensively used due to its simplicity of operation, rapid detection, low-cost, and micro-portable feature [14–16]. Typically, fiber optic sensing technology is extensively utilized in diverse fields, such as healthcare, civil infrastructure, biochemistry, and environmental monitoring [17–19]. Especially, fiber-optic surface plasmon resonance (SPR) sensors have also been widely used for heavy metal ions detection because of exceptional qualities like high resistance to electromagnetic interference, easy integration, high sensitivity, excellent flexibility, and remote sensing [20–24]. Generally, fiber SPR sensors need to be modified with specific aptamers or materials to detect different heavy metal ions, while electrochemical sensors can identify different metal ions but may require modification with sensitizing materials to enhance sensitivity. In traditional single electrochemical detection, due to the influence of background current (reduction of oxygen and precipitation of hydrogen), the background current is superimposed on the stripping current, which is difficult to deduct from the stripping current, thus limiting the sensitivity of low-concentration metal ions detection. While the SPR sensor is sensitive only to changes in the refractive index at the surface, the reduction of oxygen in the solution has little effect on the signal, and the precipitation of hydrogen is released from the electrode surface immediately, which will not have a large impact on the signal [25]. The combination of SPR and electrochemistry technology can subtract the background current from the Faraday current, greatly improving the sensitivity. In addition, the SPR sensor is sensitive to non-electroactive substances that cannot be directly detected by a single electrochemical method, making it possible to detect the entire electrochemical process in real-time. Therefore, various rapid, heightened sensitivity and reliable detection methods have been widely concerned, especially dual-mode detection.

Regarding dual-mode detection for electrochemical and plasmonic coupling, Wang et al. [26] demonstrated a quantitative form of electrochemical SPR to study electrochemical reactions by simultaneously measuring changes in electrochemical current and SPR change in the redox reaction of hexaammineruthenium (III) chloride. However, the system needs a heavy prism structure and is not preferable for portable analytical instrumentation. Li et al. [27] proposed a dual detection method of heavy metal ions based on localized SPR and anodic stripping voltammetry (ASV). The experimental results demonstrate that this method has a higher signal-to-noise ratio than a single electrochemical measurement. However, the preparation of this nano-Lycurgus cup array is complex, and the device is difficult to reach in tight space locations. Si et al. [28] reported a tilted fiber Bragg grating (TFBG)-based electrochemical SPR fiber-optic sensor for Pb^{2+} detection. The sensing probe is tiny in size. Nevertheless, as the TFBG is sensitive to polarization, the system generally needs to be firmly fixed on an optical table. Also, the sensor operates in the communication band, and the light source and the spectrometer are bulky and costly.

Herein, we propose a dual-mode detection method based on an electrochemical-SPR fiber sensor. The sensor used a multimode fiber-single mode fiber (MMF-SMF) reflection probe with a nanoscale gold film on the outer surface to excite the SPR, which also as a working electrode due to the excellent conductivity of the gold film. The SPR fiber sensor can provide real-time detection of the electrochemical process as the heavy metal ions deposition and stripping processes take place on the surface of the gold nanofilm. The experimental results demonstrate that not only separate detection of Pb^{2+} and Cu^{2+} can be achieved, with a concentration ranging from 10^{-12} to 10^{-7} M, but the different ions in the mixed solution can be distinguished.

2 Method and system

2.1 Dual-mode fiber sensing principle

Figure 1(a) shows the principle of electrochemical-SPR dual-mode metal ions detection based on a compact fiber probe. The probe consists of a section of MMF, a section of SMF, a thin gold nanofilm on the fiber surface, and a gold mirror on the end-facet. Due to the core mismatch between the MMF and SMF, an abundance of cladding modes can be excited in the SMF [29]. Hence, the SPR effect on the gold nanofilm can be excited by the evanescent wave of the cladding modes when the phase-matching condition is satisfied [30]. The SPR effect can be utilized to monitor minute refractive index changes on the surface of the gold film.

Owing to the excellent conductivity of the gold nanofilm, the fiber sensing probe can also be employed as a working electrode to perform electrochemical measurements. The typical differential pulse anodic

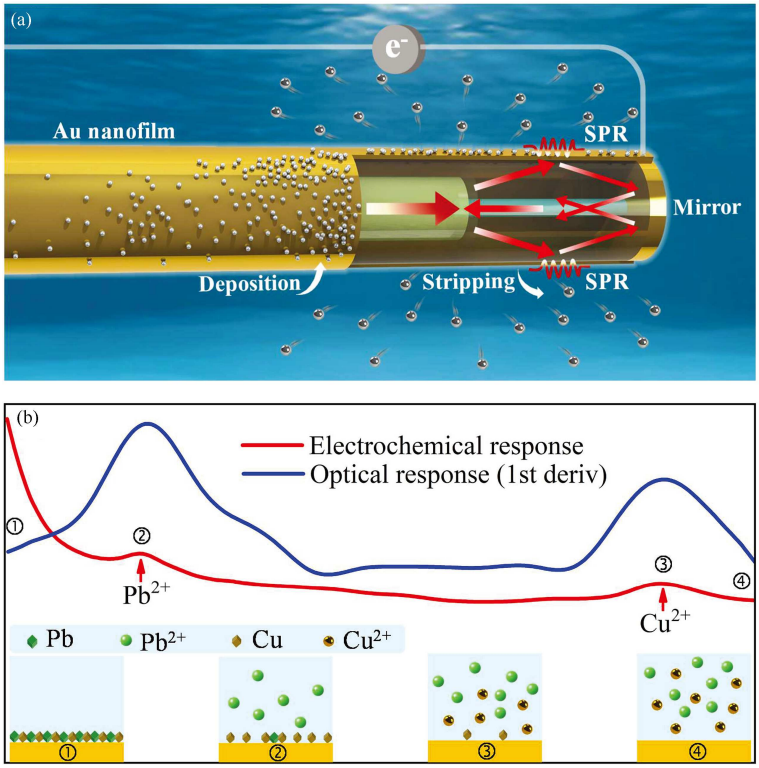

Figure 1 (Color online) (a) Schematic diagram of electrochemical-SPR dual-mode detection based on the MMF-SMF reflection structure; (b) mapping of electrochemical and optical responses during stripping.

stripping voltammetry (DPASV) method is adopted in the electrochemical process because of its fast response time and high sensitivity [31]. The DPASV process is mainly divided into two reversible processes: electrochemical deposition and stripping [32]. During the deposition process, the heavy metal ions gain electrons and undergo a reduction reaction to become metal monomers and attached to the gold nanofilm. During the stripping process, the metal monomers lose electrons and undergo an oxidation reaction, constantly stripping off from the gold nanofilm. As the SPR sensing probe is sensitive to local changes on the surface of the gold nanofilm, the whole electrochemical deposition and stripping process that happens therein can be monitored optically in real-time, enabling dual-mode analysis of the electrochemical process.

Typically, different metal ions exhibit distinct stripping potentials during the stripping process. Thus, multi-metal ions can be discriminated using the dual-mode detection method. Figure 1(b) shows the principle for two types of ion detection. There are four steps from left to right, which indicate the beginning of stripping, the characteristic stripping peak of Pb^{2+}, the characteristic stripping peak of Cu^{2+}, and the end of stripping, respectively. This method can perform in-depth dynamic analysis of the electrochemical process simultaneously via both electrochemical detection and optical analysis.

2.2 Experimental setup

The electrochemical-SPR dual-mode *in situ* detection system is shown in Figure 2. It mainly consists of two parts: the electrochemical module and the optical module. The electrochemical setup is a conventional three-electrode system, with the sensing probe functions as the working electrode, a platinum wire as the counter electrode, and an Ag/AgCl electrode as the reference electrode, respectively. An electrochemical workstation (CHI 760E, Shanghai Chen Hua Instruments Co., Ltd., China) was used to measure the electrochemical signals. The optical part contains a broadband light source and a spectrometer (Firefly 4000, Changchun New Industries Optoelectronics Technology, wavelength range 350–1000 nm), which are linked to the sensing probe through a Y-type optical fiber coupler. In addition, it should be noted that all experiments were performed under the condition of constant temperature at room temperature.

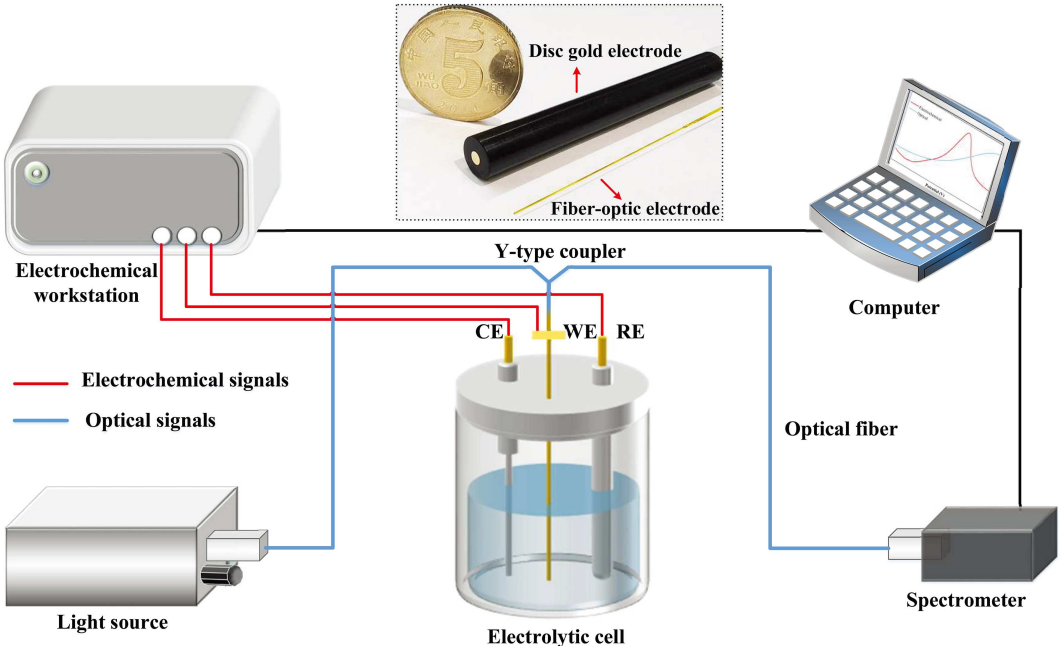

Figure 2 (Color online) Schematic illustration of the experimental setup of the electrochemical plasmonic dual-mode real-time detection system. Inset: physical comparison of the fiber-optic electrode and disc gold electrode.

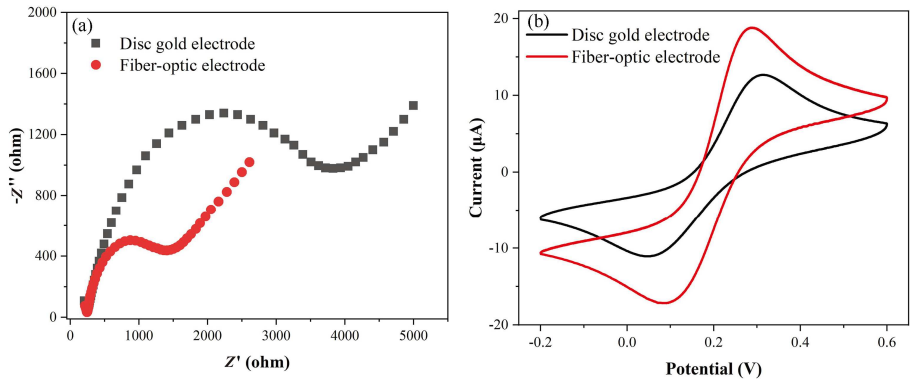

Figure 3 (Color online) (a) Nyquist diagram comparison of the fiber-optic electrode and disc gold electrode; (b) CV curves for fiber-optic electrode and disc gold electrode.

2.3 Fabrication and characterization of the dual-mode fiber sensing probe

The sensing probe is fabricated via a series of procedures. First, a section of SMF (SMF28e, Core/cladding diameter: 8.2/125 μm, Coning) is spliced with a section of MMF (MMF-S105/125-22A, Core/cladding diameter: 105/125 μm, Nufern), and then the SMF is cut to a desired length (10 mm). Second, the end facet of the fiber probe is coated with about 300 nm-thick gold film to form a reflection mirror by the magnetron sputtering method. Last, the outer surface of the fiber probe is coated with a 50 nm-thick gold nanofilm using a magnetron sputtering machine. The detailed coating procedure can be found in our previous work [33,34]. As shown in Figure 2 (inset), the footprint and size of the fiber-optic electrode are much smaller than the conventional disc gold electrode.

Electrochemical impedance spectroscopy (EIS) can evaluate the resistance and electron transport capability of a working electrode [35]. The EIS parameters are set as follows: amplitude of 5 mV, potential of 0.212 V, and frequency range of 1–10^5 Hz. As shown in Figure 3(a), the Nyquist radius of the fiber-optic electrode is significantly smaller than that of the disc electrode. Namely, the fiber-optical electrode has a better electron transport ability, mainly due to the larger electroactive surface area of the fiber-optic electrode. The size of the fiber-optic electrode inserted into the solution is 125 μm × 20 mm (diameter × length), which provides a significantly larger electroactive surface area than the conventional disc electrode with a 2 mm diameter. EIS and cyclic voltammetry (CV) measurements were carried out in the

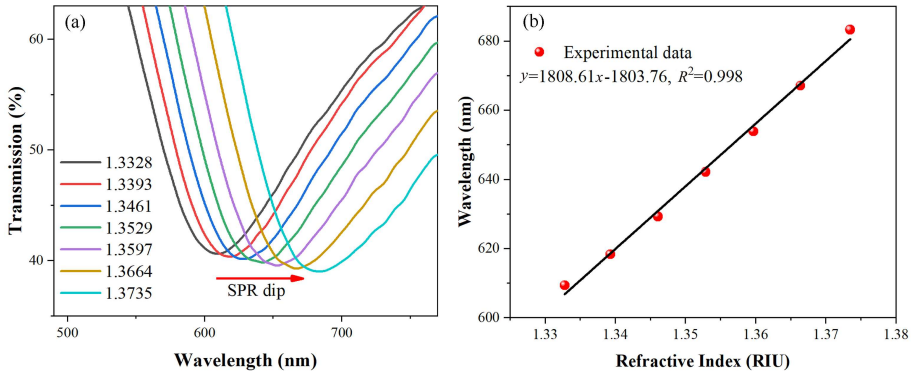

Figure 4 (Color online) (a) SPR transmission spectra with different refractive indices; (b) linear fitting curve of wavelength variation.

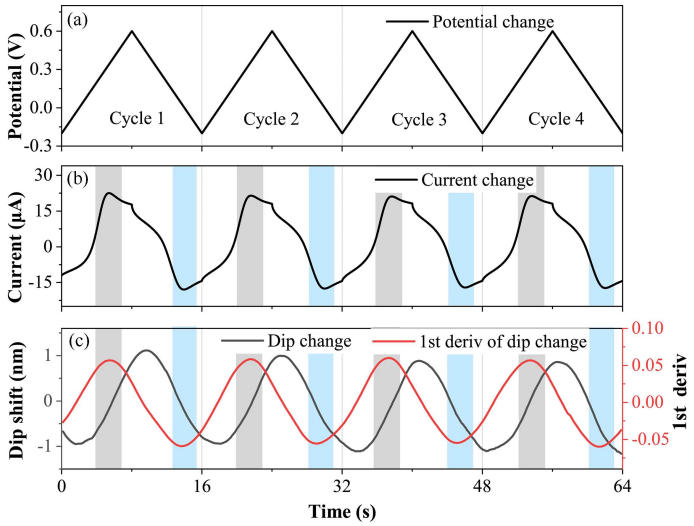

Figure 5 (Color online) (a) Electrochemical potential change for four CV cycles; (b) current change of the sensor during the CV process; (c) corresponding spectral wavelength variation during the CV process.

electrolyte of 5 mM $[Fe(C.N.)_6]^{3-/4-}$ and 0.1 M KCl. As shown in Figure 3(b), the response potential of CV is −0.2–0.6 V, and the scanning rate is 0.1 V/s. It can be observed that the fiber-optic electrode is similar to the disk electrode, with a pair of reversible redox peaks. Additionally, the fiber-optic electrode exhibits higher current intensity in the CV curve primarily due to its superior electronic transfer ability.

In addition, to detect the wavelength sensitivity of the fiber sensor probe (SMF length is 10 mm), the refractive index calibration was performed in sodium chloride (NaCl) solution. The refractive index ranges from 1.3328 to 1.3735, calibrated by a refractometer. As shown in Figure 4(a), the spectra exhibit a typical SPR dip phenomenon, and the wavelength is redshifted with the increase of the refractive index. Figure 4(b) depicts the sensitivity fitting curves for the wavelength change. The wavelength sensitivity is 1808.61 nm/RIU, and the correlation coefficient (R^2) exceeds 0.99.

Furthermore, CV tests were performed to investigate the correspondence between electrochemical and spectral responses. As shown in Figure 5(a), the potential of CV varies from −0.2 to 0.6 V (four cycles at a scan rate of 0.1 V/s). Figure 5(b) depicts the current variation of the sensor during the CV process, with the gray area and blue area representing the oxidation and reduction peaks, respectively. As illustrated in Figure 5(c), the black line is the wavelength dip change, and the red line shows the first derivative of the wavelength response, with the positive peak corresponding to the oxidation peak (gray area) and the negative peak corresponding to the reduction peak (blue area), respectively. It can be seen that the spectral response can reflect the electrochemical change rate in real-time.

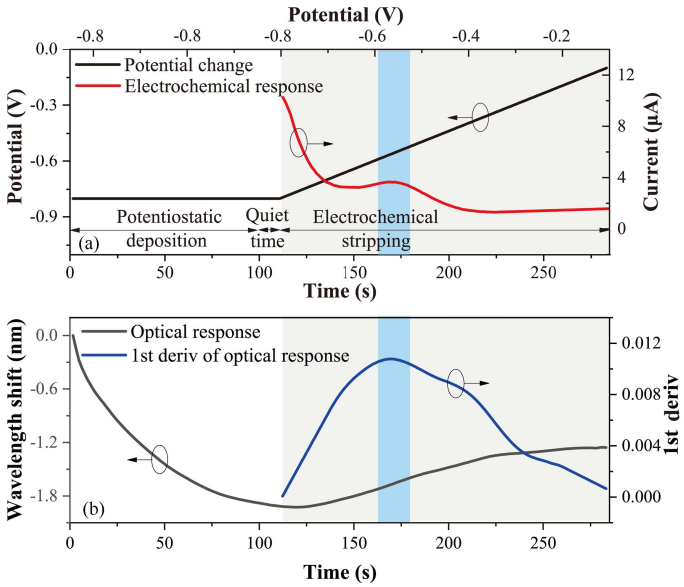

Figure 6 (Color online) Optical and electrochemical mapping relationship (taking 10^{-9} M as an example). (a) Correspondence between electrochemical response and scanning potential throughout the DPASV process; (b) optical response of the entire DPASV process and its first-order derivative in the stripping process.

2.4 Materials

Lead acetate [$Pb(CH_3COO)_2 \cdot 3H_2O$], Copper(II) acetate monohydrate ($C_4H_6CuO_4{\cdot}H_2O$), acetic acid (CH_3COOH, HAc), and sodium acetate trihydrate ($CH_3COONa \cdot 3H_2O$, NaAc) were purchased from Shanghai Aladdin Biochemical Technology Co., Ltd. All reagents are of analytical grade and require no further purification. Ultrapure water (18 MΩ·cm) was used in all buffer and solvent configurations. Moreover, a weakly acidic buffer (pH 4.5, calibrated with a pH meter) was prepared from acetic acid and sodium acetate.

3 Experimental results and discussions

3.1 Electrochemical and optical responses of Pb^{2+}

The DPASV method is employed in electrochemical detection with the following key parameters: −0.8 V for the deposition potential, 100 s for the deposition duration, 10 s for the quiet time, 1 s for the pulse period, and scanning potential ranging from −0.8 to 0.1 V (optimized parameters derived from many experiments). Figure 6(a) shows the corresponding relationship between the electrochemical potential change and electrochemical response. No electrochemical response can be recorded during the potentiostatic deposition process (i.e., the "black box" process of electrochemical deposition).

Figure 6(b) shows the corresponding optical responses during the entire DPASV process and the first-order derivative of the optical response during the stripping process. The SPR wavelength blueshifts rapidly and then gradually levels off during the deposition at a constant potential of −0.8 V. This is mainly because the lead ions are continually reduced into lead monomers and plated onto the surface of the gold nanofilm-coated fiber in the electrochemical deposition process, causing the refractive index of the sensing surface to change. During the electrochemical stripping process (light gray area), the spectrum remains almost constant at the beginning of the stripping. It then gradually increases when the potential reaches the point where the lead monomers start to be stripped out. This is primarily caused by the continuous oxidation and stripping out of the lead monomers from the fiber's surface, causing a change in the refractive index at the interface, which is reflected in the redshift of the spectral wavelength. When the Pb^{2+} characteristic stripping peak potential is reached, namely the metal ions are stripped out from the electrode surface at the maximum rate, and the corresponding spectrum change is the fastest. It is also proved by experiments that the first-order derivative of the wavelength response is consistent with the electrochemical characteristic stripping peak (blue area).

Figures 7(a)–(d) indicate the electrochemical and optical experimental results and fitting curves of

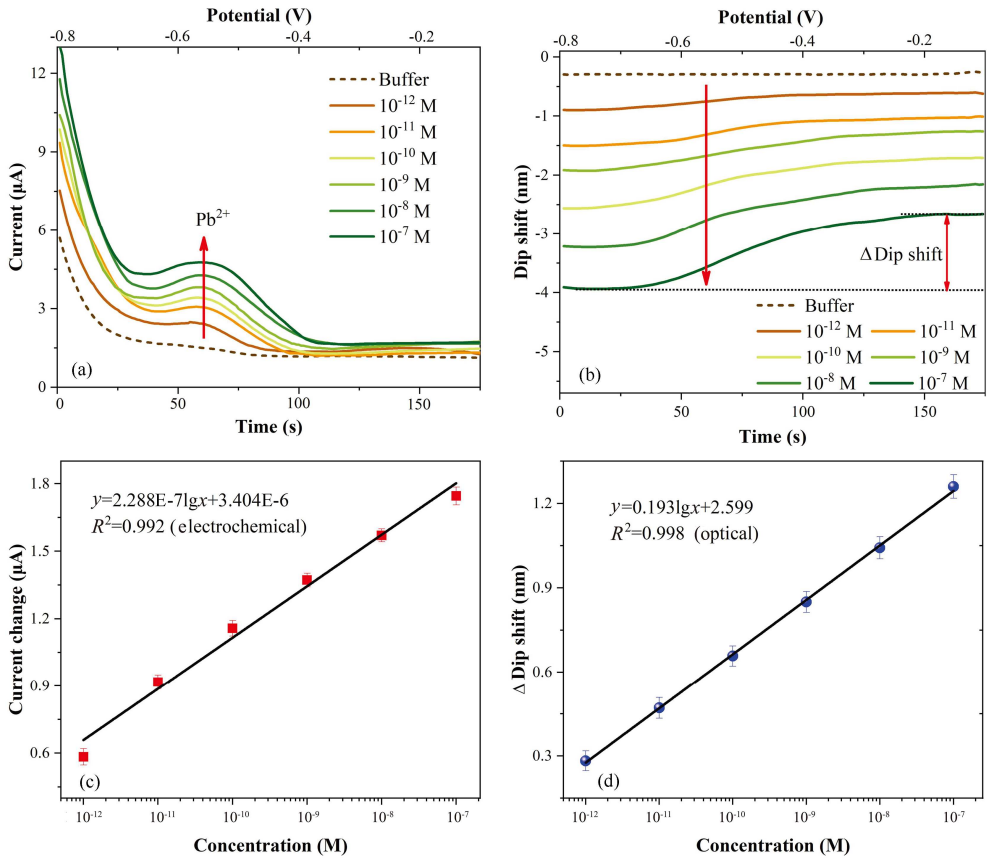

Figure 7 (Color online) Evolution of the electrochemical and optical response of Pb^{2+} concentration ranging from 10^{-12} to 10^{-7} M. (a) Electrochemical response results; (b) optical spectrum wavelength response results; (c) linear fitting plots at different concentrations of electrochemistry; (d) linear fitting plots of optics at different concentrations.

Pb^{2+} concentration ranging from 10^{-12} to 10^{-7} M. The electrochemical response results are shown in Figure 7(a). It can be seen that the current increases gradually as the Pb^{2+} concentration increases. Additionally, the stripping peak potential is approximately −0.56 V, corresponding to the classic characteristic stripping peak of Pb^{2+} [36]. It is worth noting that *i*-*t* electrochemical cleaning is performed with deionized water after each detection. Under high electrical potential, the metal monomers can undergo oxidation and be stripped from the electrode surface into the deionized water. Figure 7(b) displays the synchronized optical response results during the stripping process. It can be found that the amount of change in the wavelength shift (Δdip shift) increases with increasing concentration. As shown in Figure 7(c), it is the linear fitting curve of the electrochemistry. The correlation function is $y = 2.288\text{E} - 7 \lg x + 3.404\text{E} - 6$, $R^2 = 0.992$ (x: concentration (M), y: current (A)). The detection performance was evaluated by the limit of detection (LOD), calculated as $\text{LOD} = 10^{(3\text{Sa}-y(0))/a}$, where Sa is the standard deviation of the blank buffer (three measurements) and a is the sensitivity (slope) [37]. Thus, the LOD is about 1.69×10^{-14} M, significantly below the EPA-specified maximum permitted level for Pb^{2+}. The linear fitting curve of the optical response is shown in Figure 7(d). The correlation function is $y = 0.193 \lg x + 2.599$, $R^2 = 0.998$ (x: concentration (M), y: Δdip shift (nm)), and the LOD is about 5.49×10^{-13} M.

3.2 Electrochemical and optical responses of Cu^{2+}

The specific electrochemical setup's critical parameters are as follows: enrichment potential of −0.2 V, deposition duration of 100 s, quiet time of 10 s, and stripping potential changes from −0.2 to 0.5 V. Again, to illustrate the relationship between electrochemical scanning potential and electrochemical response, the correspondence is plotted in Figure 8(a). The optical response of the entire electrochemical process and its first-order derivative in the stripping process is shown in Figure 8(b). The results show that the changing pattern is consistent with Pb^{2+}.

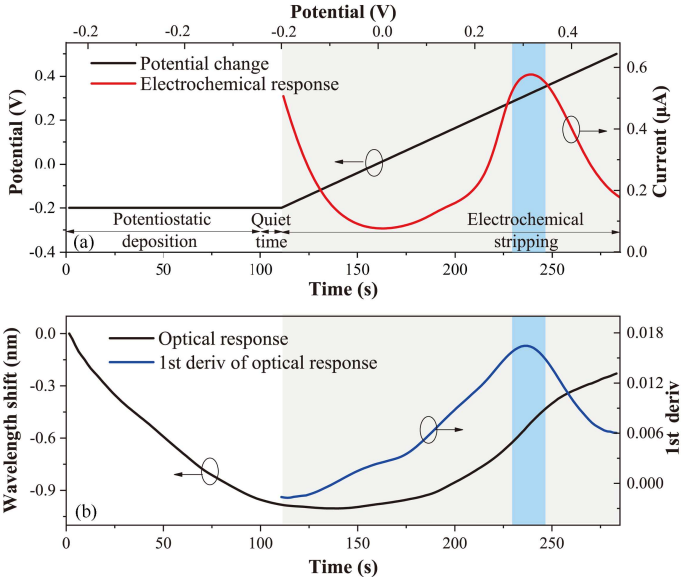

Figure 8 (Color online) Correspondence between optical and electrochemical responses (Cu^{2+} concentration at 10^{-9} M). (a) The relationship between electrochemical response and scanning potential during the entire electrochemical process; (b) the optical response of the entire electrochemical process and its first-order derivative in the stripping process.

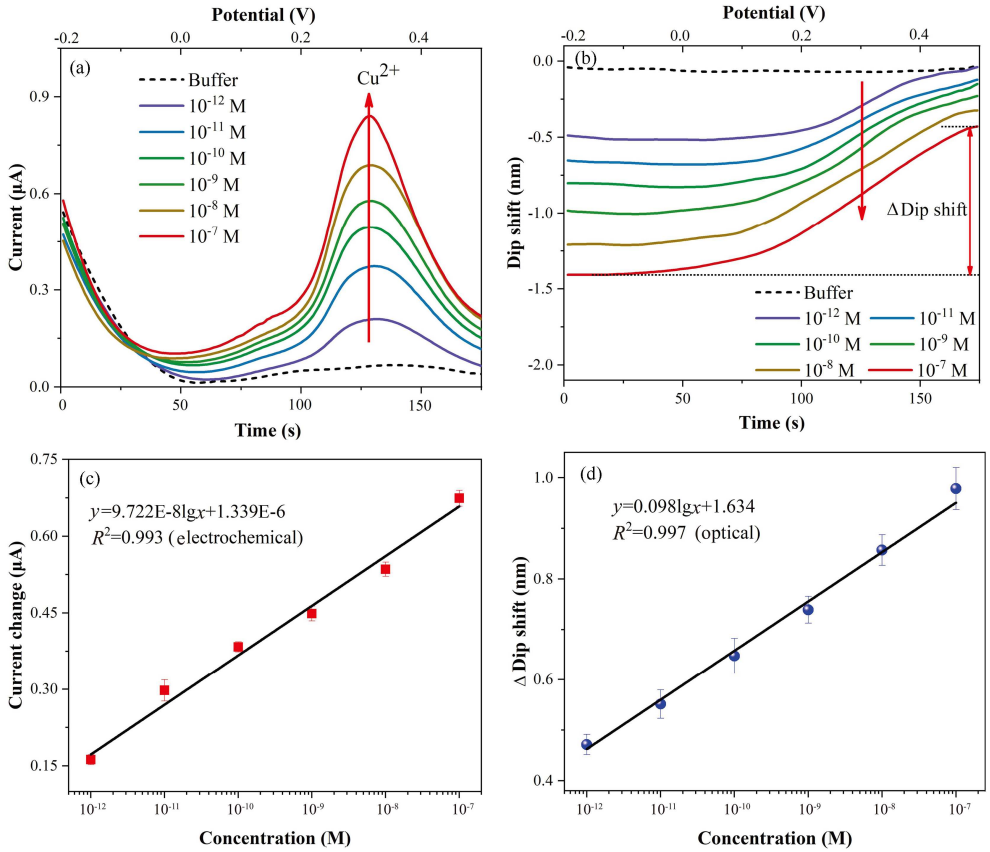

Figure 9 (Color online) Evolution of the electrochemical and optical responses for Cu^{2+} concentration ranging from 10^{-12} to 10^{-7} M. (a) Electrochemical response results; (b) results of the spectral wavelength response in the stripping process; (c) linear fitting curves for different concentrations of electrochemistry; (d) linear fitting curves for different concentrations of optics.

As shown in Figure 9(a), the current intensity gradually rises along with the Cu^{2+} concentration (10^{-12}–10^{-7} M). The potential of the stripping peak is roughly 0.31 V, corresponding to the normal characteristic peak of Cu^{2+}. Figure 9(b) shows the synchronized optical response results in the stripping

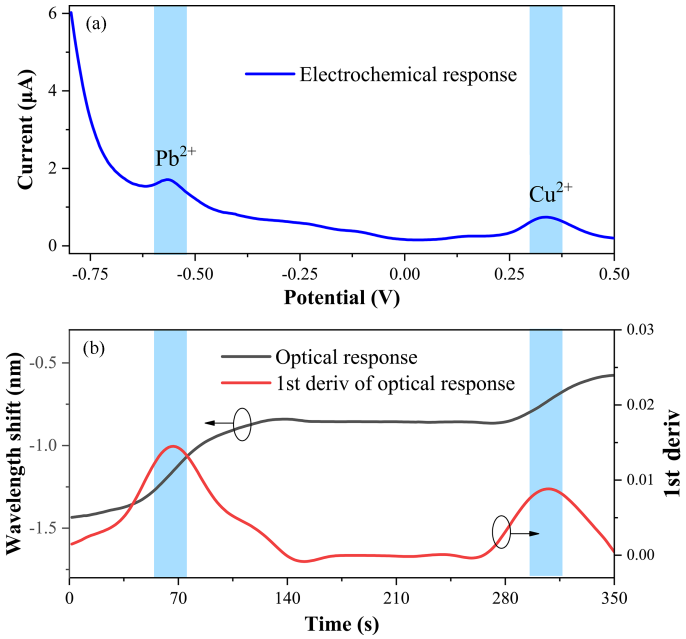

Figure 10 (Color online) Simultaneous detection of mixed Pb^{2+} and Cu^{2+} solutions using the plasmonic & electrochemical dual-mode approach. (a) Electrochemical response curve; (b) optical response curve and the first-order differentiation of the optical response.

Table 1 Comparison of different detection methods for heavy metal ions

Methods	Modified materials	Sensors	Detection target ions	LODs (M) [38]	Refs.
Optical	L-glutathione	Microfiber	Pb^{2+}	1.32×10^{-8}	[12]
Optical	Gold nanoparticles, DNAzyme	TFBG	Pb^{2+}	8.56×10^{-12}	[24]
Electrochemical	Metal-free g-C_3N_4, carbon black	Glassy carbon electrode	Cd^{2+}, Pb^{2+}, Hg^{2+}	$0.22–2.10\times10^{-9}$	[31]
Electrochemical	Fe_3O_4@PDA-DMSA	Glassy carbon electrode	Pb^{2+}, Cu^{2+}	$0.26–1.00\times10^{-9}$	[16]
Localized SPR and electrochemical	Gold nanoparticles array	Microchip	Zn^{2+}, Pb^{2+}, Cu^{2+}	NA	[27]
Plasmonic & electrochemical dual-mode	Not required	MMF-SMF fiber	Pb^{2+}, Cu^{2+}	$0.16–5.49\times10^{-13}$	This work

process. The pattern of change in the response curve indicates that it is similar to the detection of Pb^{2+}. The electrochemical linear fitting curve is shown in Figure 9(c), and the function is $y = 9.722\text{E} - 8\lg x + 1.339\text{E} - 6$, $R^2 = 0.993$ (x: concentration (M), y: current (A)). So, the LOD is approximately 2.75×10^{-14} M, far below the maximum permitted level for Cu^{2+} specified by EPA. Moreover, the optical linear fitting curve is depicted in Figure 9(d). The correlation function is $y = 0.098\lg x + 1.634$, $R^2 = 0.998$ (x: concentration (M), y: Δdip shift (nm)), and the LOD is about 5.01×10^{-14} M.

3.3 Simultaneous detection of multi-metal-ions

Typically, each heavy metal ions sensor needs to demonstrate its specificity, that is, the ability to distinguish between different ions in a mixed solution. During constant potential deposition, metal ions gain electrons to metal monomers, and different metal monomers are selectively stripped off during forward scanning potential. Figure 10 shows the detection result of the mixed solution of Pb^{2+} and Cu^{2+} (the concentration of both solutions is 10^{-9} M, and the volume ratio is 1 : 1). As shown in Figure 10(a), the characteristic stripping peaks of Pb^{2+} and Cu^{2+} are -0.56 and 0.31 V, respectively, which agrees well with the results of the individual measurements. The corresponding optical response is shown in Figure 10(b), and a first-order differentiation is performed to better reflect the optical response variation. This result indicates that for the two different heavy metal ions, the rate of wavelength response is not constant during stripping and is closely related to the characteristic stripping peaks of the different

heavy metals. It can be seen that the first-order derivative of the spectral response corresponds to the characteristic stripping peak potential of the electrochemical response (blue area).

Finally, the comparison of optical or electrochemical methods for the detection of heavy metal ions is shown in Table 1. It can be seen that the proposed dual-modal detection method using MMF-SMF compact reflective probe does not require complex modification and can achieve multiple heavy metal ions measurements with low LOD values.

4 Conclusion

In this work, we propose the plasmonic & electrochemical dual-mode fiber sensing probe to detect multiple heavy metal ions. The sensing probe comprises an MMF-SMF reflector and a gold nanofilm on the outer surface. It can detect minute refractive index variations at the gold nanofilm-liquid interface via the SPR effect while acting as the working electrode, enabling simultaneous detection of electrochemical and optical responses. Pb^{2+} and Cu^{2+} can not only be detected individually but also identified in mixed solutions. The dual-mode sensor can perform real-time detection of the entire electrochemical process so that the electrochemical and optical information can complement each other and improve the anti-interference ability. The proposed fiber sensor is modification-free and label-free and can be mass-fabricated, making it intensely convenient for one-time use to avoid cross-contamination, creating a multitude of opportunities for complex and hazardous environment detection.

Acknowledgements This work was supported in part by National Natural Science Foundation of China (Grant Nos. 62035006, 61975068, 62005101, 61827819), Guangdong Outstanding Scientific Innovation Foundation (Grant No. 2019TX05X383), Program of Marine Economy Development Special Fund under Department of Natural Resources of Guangdong Province (Grant No. GDNRC [2023]23), Local Innovative and Research Teams Project of Guangdong Pearl River Talents Program (Grant No. 2019BT02X105), Research Fund of Guangdong-Hong Kong-Macao Joint Laboratory for Intelligent Micro-Nano Optoelectronic Technology (Grant No. 2020B1212030010), Project of Scientific and Technological Development Plan of Jilin Province (Grant No. 20220508130RC), and Open Fund of Guangdong Provincial Key Laboratory of Optical Fiber Sensing and Communication Technology.

References

1 Mourya A, Sinha S K, Mazumdar B. Glassy carbon electrode modified with blast furnace slag for electrochemical investigation of Cu^{2+} and Pb^{2+} metal ions. MicroChem J, 2019, 147: 707–716
2 Valko M, Jomova K, Rhodes C J, et al. Redox- and non-redox-metal-induced formation of free radicals and their role in human disease. Arch Toxicol, 2016, 90: 1–37
3 Zhang M, Sun X, Xu J L. Heavy metal pollution in the East China Sea: a review. Mar Pollution Bull, 2020, 159: 111473
4 Vardhan K H, Kumar P S, Panda R C. A review on heavy metal pollution, toxicity and remedial measures: current trends and future perspectives. J Mol Liquids, 2019, 290: 111197
5 Liu X L, Wang Y Z, Song Y J. Visually multiplexed quantitation of heavy metal ions in water using volumetric bar-chart chip. Biosens Bioelectron, 2018, 117: 644–650
6 Ghaedi M, Fathi M R, Shokrollahi A, et al. Highly selective and sensitive preconcentration of mercury ion and determination by cold vapor atomic absorption spectroscopy. Anal Lett, 2006, 39: 1171–1185
7 Li W W, Liu J, Sun K, et al. Highly fluorescent water soluble $Cd_xZn_{1-x}Te$ alloyed quantum dots prepared in aqueous solution: one-step synthesis and the alloy effect of Zn. J Mater Chem, 2010, 20: 2133–2138
8 Rasheed T, Bilal M, Nabeel F, et al. Fluorescent sensor based models for the detection of environmentally-related toxic heavy metals. Sci Total Environ, 2018, 615: 476–485
9 Kumar M K, Nagendrappa G, Shivanna A M. ICP-AES estimation of a few heavy and toxic metal ions present in water samples collected from the three lakes situated in Bangalore city. Environ Sci Technol, 2016, 15: 549
10 Karami H, Mousavi M F, Yamini Y, et al. On-line preconcentration and simultaneous determination of heavy metal ions by inductively coupled plasma-atomic emission spectrometry. Anal Chim Acta, 2004, 509: 89–94
11 Cocherie A, Robert M. Direct measurement of lead isotope ratios in low concentration environmental samples by MC-ICP-MS and multi-ion counting. Chem Geol, 2007, 243: 90–104
12 Yap S H K, Chien Y H, Tan R, et al. An advanced hand-held microfiber-based sensor for ultrasensitive lead ion detection. ACS Sens, 2018, 3: 2506–2512
13 Lu M D, Zhou H F, Peng W, et al. Dithiol self-assembled monolayer based electrochemical surface plasmon resonance optical fiber sensor for selective heavy metal ions detection. J Lightwave Technol, 2021, 39: 4034–4040
14 Hwang J H, Wang X, Zhao D, et al. A novel nanoporous bismuth electrode sensor for *in situ* heavy metal detection. Electrochim Acta, 2019, 298: 440–448
15 Lee S, Oh J, Kim D, et al. A sensitive electrochemical sensor using an iron oxide/graphene composite for the simultaneous detection of heavy metal ions. Talanta, 2016, 160: 528–536
16 Wang L L, Jiang X, Su S, et al. A thiol and magnetic polymer-based electrochemical sensor for on-site simultaneous detection of lead and copper in water. MicroChem J, 2021, 168: 106493
17 Ge K, Xu Z Y, Guo D, et al. RGB WGM lasing woven in fiber braiding cavity. Sci China Inf Sci, 2022, 65: 182403
18 Hao Z, Ma Y X, Jiang B Q, et al. Second harmonic generation in a hollow-core fiber filled with GaSe nanosheets. Sci China Inf Sci, 2022, 65: 162403
19 Huang L J, He Z Y, Fan X Y. Simplified single-end Rayleigh and Brillouin hybrid distributed fiber-optic sensing system. Sci China Inf Sci, 2023, 66: 129404
20 Yanase Y, Araki A, Suzuki H, et al. Development of an optical fiber SPR sensor for living cell activation. Biosens Bioelectron, 2010, 25: 1244–1247

21 Shrivastav A M, Usha S P, Gupta B D. Fiber optic profenofos sensor based on surface plasmon resonance technique and molecular imprinting. Biosens Bioelectron, 2016, 79: 150–157
22 Cai S S, Liu F, Wang R L, et al. Narrow bandwidth fiber-optic spectral combs for renewable hydrogen detection. Sci China Inf Sci, 2020, 63: 222401
23 Wang R L, Zhang H Z, Liu Q Y, et al. Operando monitoring of ion activities in aqueous batteries with plasmonic fiber-optic sensors. Nat Commun, 2022, 13: 547
24 Wang F, Zhang Y, Lu M D, et al. Near-infrared band Gold nanoparticles-Au film "hot spot" model based label-free ultratrace lead (II) ions detection via fiber SPR DNAzyme biosensor. Sens Actuat B-Chem, 2021, 337: 129816
25 Wang S P, Forzani E S, Tao N J. Detection of heavy metal ions in water by high-resolution surface plasmon resonance spectroscopy combined with anodic stripping voltammetry. Anal Chem, 2007, 79: 4427–4432
26 Wang S P, Huang X P, Shan X N, et al. Electrochemical surface plasmon resonance: basic formalism and experimental validation. Anal Chem, 2010, 82: 935–941
27 Li N T, Zhang D M, Zhang Q, et al. Combining localized surface plasmon resonance with anodic stripping voltammetry for heavy metal ion detection. Sens Actuat B-Chem, 2016, 231: 349–356
28 Si Y, Lao J J, Zhang X J, et al. Electrochemical plasmonic fiber-optic sensors for ultra-sensitive heavy metal detection. J Lightwave Technol, 2019, 37: 3495–3502
29 Zhou S R, Li X J, Zhang J H, et al. Dual-fiber optic bioprobe system for triglyceride detection using surface plasmon resonance sensing and lipase-immobilized magnetic bead hydrolysis. Biosens Bioelectron, 2022, 196: 113723
30 Chen Z L, Han K L, Zhang Y N. Reflective fiber surface plasmon resonance sensor for high-sensitive mercury ion detection. Appl Sci, 2019, 9: 1480
31 Hu J Y, Li Z, Zhai C Y, et al. Photo-assisted simultaneous electrochemical detection of multiple heavy metal ions with a metal-free carbon black anchored graphitic carbon nitride sensor. Anal Chim Acta, 2021, 1183: 338951
32 Peng X L, Ren Z C, Lu C H, et al. Hybrid electrochemical-surface plasmon resonance microfiber sensor for Pb^{2+} detection. J Lightwave Technol, 2023, 41: 4307–4314
33 Caucheteur C, Guo T, Liu F, et al. Ultrasensitive plasmonic sensing in air using optical fibre spectral combs. Nat Commun, 2016, 7: 1–8
34 Liu F, Zhang X J, Li K W, et al. Discrimination of bulk and surface refractive index change in plasmonic sensors with narrow bandwidth resonance combs. ACS Sens, 2021, 6: 3013–3023
35 Li Z, Zhang H M, Zha Q B, et al. Photo-electrochemical detection of dopamine in human urine and calf serum based on MIL-101 (Cr)/carbon black. Microchim Acta, 2020, 187: 526
36 Pathak P, Hwang J H, Li R H T, et al. Flexible copper-biopolymer nanocomposite sensors for trace level lead detection in water. Sens Actuat B-Chem, 2021, 344: 130263
37 Liu L H, Zhang X J, Zhu Q, et al. Ultrasensitive detection of endocrine disruptors via superfine plasmonic spectral combs. Light Sci Appl, 2021, 10: 181
38 Chiavaioli F, Gouveia C, Jorge P, et al. Towards a uniform metrological assessment of grating-based optical fiber sensors: from refractometers to biosensors. Biosensors, 2017, 7: 23